Computational Study on the Aminolysis of β-Hydroxy-α,β-Unsaturated Ester via the Favorable Path Including the Formation of α-Oxo Ketene Intermediate

Lu Jin,[†] Ying Xue,*[,†,‡] Hui Zhang,[§] Chan Kyung Kim,*[,§] Dai Qian Xie,[||] and Guo Sen Yan[†]

College of Chemistry, Sichuan University, Chengdu 610064, P. R. China, State Key Laboratory of Biotherapy, Sichuan University, Chengdu 610041, P. R. China, Department of Chemistry, Inha University, Incheon 402-751, Korea and Institute of Theoretical and Computational Chemistry, Key Laboratory of Mesoscopic Chemistry, School of Chemistry and Chemical Engineering, Nanjing University, Nanjing 210093, P. R. China

Received: July 18, 2007; Revised Manuscript Received: December 29, 2007

The possible mechanisms of the aminolysis of *N*-methyl-3-(methoxycarbonyl)-4-hydroxy-2-pyridone (β-hydroxy-α,β-unsaturated ester) with dimethylamine are investigated at the hybrid density functional theory B3LYP/6-31G(d,p) level in the gas phase. Single-point computations at the B3LYP/6-311++G(d,p) and the Becke88-Becke95 1-parameter model BB1K/6-311++G(d,p) levels are performed for more precise energy predictions. Solvent effects are also assessed by single-point calculations at the integral equation formalism polarized continuum model IEFPCM-B3LYP/6-311++G(d,p) and IEFPCM-BB1K/6-311++G(d,p) levels on the gas-phase optimized geometries. Three possible pathways, the concerted pathway (path A), the stepwise pathway involving tetrahedral intermediates (path B), and the stepwise pathway via α-oxo ketene intermediate due to the participation of β-hydroxy (path C), are taken into account for the title reaction. Moreover, path C includes two sequential processes. The first process is to generate α-oxo ketene intermediate via the decomposition of *N*-methyl-3-(methoxycarbonyl)-4-hydroxy-2-pyridone; the second process is the addition of dimethylamine to α-oxo ketene intermediate. Our results indicate that path C is more favorable than paths A and B both in the gas phase and in solvent (heptane). In path C, the first process is the rate-determining step, and the second process is revealed to be a [4+2] pseudopericyclic reaction without the energy barrier. Being independent of the concentration of amine, the first process obeys the first-order rate law.

1. Introduction

The aminolysis reaction of esters is a fundamental process in both organic and biological chemistry and its mechanism has long been of great interest in the experimental and theoretical investigations.[1–20] Conceptually, there are three possible reaction mechanisms for the bimolecular aminolysis reaction of esters in literatures. The first one is the concerted mechanism in which the formation of two new bonds and the cleavage of two old bonds simultaneously happen via one step, the second is the stepwise mechanism involving neutral intermediates via the addition and elimination steps, and the third mechanism includes zwitterionic intermediates in the reaction. For some reactions of ester aminolysis, it failed to locate zwitterionic intermediates with computational methods and found that the addition/elimination stepwise mechanism and the concerted mechanism have very close activation energy barriers, both of which are so high that the reaction could occur neither at room temperature nor without a catalyst.[7,9,17] The results also showed that the rate-limiting step is to form the four-membered ring transition state for the concerted mechanism or the tetrahedral intermediate for the addition/elimination stepwise mechanism. In the case of the four-membered ring transition state in the concerted process, amine attacks on carbonyl group, followed by a proton shift from amine to ester, whereas for the tetrahedral intermediates in the addition/elimination stepwise process, amine has attached at the C atom of carbonyl and a proton has also transferred from amine to the O atom of carbonyl, rendering that the C═O double bond of carbonyl has been broken and that the hybridization of C atom of carbonyl has changed from sp^2 to sp^3 to form a tetrahedral carbon.

SCHEME 1: Equilibrium between 1 and 2 via α-Oxo Ketene 3

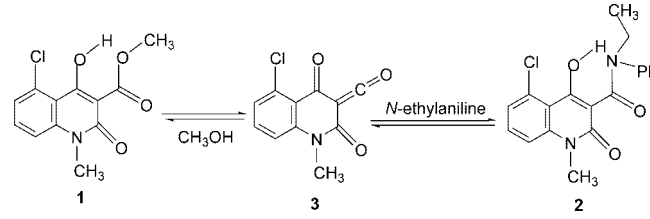

The high reaction energy barrier needs a high reaction temperature. So, for the aminolysis of esters, in that the unexpected side reactions can be activated at high temperature, amides are produced in low yield in many cases. Recently, as shown in Scheme 1, Jansson et al.[21] reported a high-yielding aminolysis reaction of 5-chloro-4-hydroxy-1-methyl-2-oxo-1,2-dihydro-3-(carboxylic acid methyl ester)quinoline (**1**) with *N*-ethylaniline in heptane. They proposed that the equilibrium exists between **1** and 5-chloro-1,2-dihydro-4-hydroxy-1-methyl-2-oxo-3-(*N*-ethyl-*N*-phenyl-carboxamide)quinoline (**2**) due to the participation of β-hydroxy in the aminolysis reaction, and that the removal of formed methanol is a prerequisite for obtaining **2** from **1**in high yield in the reaction. The equilibrium is probably maintained via α-oxo ketene intermediate 5-chloro-1-methyl-

* Corresponding authors. Y.X.: e-mail, xueyingscu@163.com; tel, +86-28-85418330; fax, +86-28-85575569. C.K.K: e-mail, kckyung@inha.ac.kr; tel, +82-32-8607684; fax, +82-32-8675604.
[†] College of Chemistry, Sichuan University.
[‡] State Key Laboratory of Biotherapy, Sichuan University.
[§] Inha University.
[||] Nanjing University.

10.1021/jp0756496 CCC: $40.75
Published on Web 04/11/2008

SCHEME 2: Possible Reactions with α-Oxo Ketene

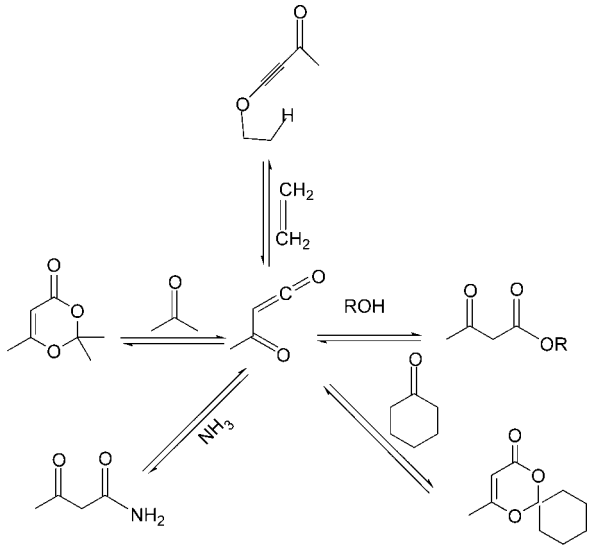

2,4-dioxo-1,2,3,4-tetrahydro-3-methanonequinoline (**3**) rather than the four-membered ring transition state or the tetrahedral intermediate. In their experiment, they had made several attempts to isolate α-oxo ketene **3**, but none was successful. The kinetic study strongly revealed that the reaction obeys the first-order rate law which is independent of the concentration of *N*-ethylamine.

α-Oxo ketenes, with an in-plane lone pair of α-oxygen and a C═O double bond in conjugation with ketene, are an important subject of experimental[22–32] and theoretical[33–46] chemistry. Being interesting structural features, high reactivity, and synthetic utility, α-oxo ketenes have been extensively investigated in the past decades. As reactive intermediates, α-oxo ketenes can be thermally and photochemically generated in the pharmaceutical, agrichemical, chemical, and polymer industries and are also identified in solution and argon matrix in some reactions. Of these reactions of α-oxo ketenes, Birney et al. have focused on the unusual reactivity of α-oxo ketenes as a four-center partner in [4+2] reactions,[33–35] which occur at C═C double bond of ketenes and α-position C═O double bond, against the most common [2+2] reactions of typical ketenes,[47–60] which occur at the C═C double bond of ketenes. Birney et al. confirmed that transition states for [4+2] reactions between α-oxo ketenes and nucleophiles, such as water and amines, are approximately planar and that this concerted process is considered as a pseudopericyclic reaction.[35] A pseudopericyclic reaction, coined by Lemal et al., is a concerted transformation whose primary changes in bonding compass a cyclic array of atoms, at one (or more) of which, the nonbonding and bonding atomic orbitals interchange roles.[61]

When 1,3-dioxin-4-ones, the enol of β-keto esters or ethoxybutynone was heated in the presence of a variety of trapping agents, such as alcohols, ketones, alkenes and amines, identical products were obtained (Scheme 2). The trend in reactivities of these reactants follows the general order: amines > alcohols >> aldehydes ≈ ketones, which can be rationalized by considering both the nucleophilicity and electrophilicity of the reacting species. Spectroscopic and kinetic studies indicated that these transacetoacetylation reactions proceed via the mechanism in which α-oxo ketene is at first formed in the rate-limiting unimolecular decomposition step which is independent of the nature of the nucleophile, followed by the reaction of this intermediate with a nucleophile. In the absence of trapping agents, although α-oxo ketenes will undergo dimerization, this reaction is also reversible. Because α-oxo ketenes react rapidly with both the added nucleophile and the co-product cleaved from the reactants, these reactions, on the preparative scale, are essentially carried out by refluxing the reactants and an excess of the nucleophile. It was found that the reactions show no appreciable solvent effect without an added catalyst in nonpolar solvents, such as xylene and toluene.

Up to now, many theoretical studies on [2+2] reactions of typical ketenes were comprehensively reported,[56–60] whereas few of [4+2] reactions of α-oxo ketenes with alcohol, formaldehyde, or amines have been investigated with theoretical methods. To our best knowledge, the mechanism of the aminolysis of β-hydroxy-α,β-unsaturated ester via α-oxo ketene intermediate is not totally clear until now. We think it is very interesting to make clear this mechanism. To match with the experiment[21]and consider the cost of calculations, *N*-methyl-3-(methoxycarbonyl)-4-hydroxy-2-pyridone and dimethylamine were selected as our computational models to study the reaction mechanism. Therefore, in this study, our motif is mainly focused on the clarification of the mechanism for the aminolysis of *N*-methyl-3-(methoxycarbonyl)-4-hydroxy-2-pyridone (β-hydroxy-α,β-unsaturated ester) with dimethylamine. Three possible reaction pathways (Scheme 3) are studied in detail using quantum chemical methods. In addition, solvent effects in heptane are also examined with the self-consistent reaction field (SCRF) method.

2. Computational Details

All of calculations were carried out with the Gaussian 03 program package.[62] The relevant stationary points (reactant complexes, intermediates, transition states, and product complexes) were fully optimized in the gas phase, using the hybrid density functional theory (B3LYP)[63–65] in conjunction with the 6-31G(d,p) basis set. Stationary points were further characterized by analytic computations of harmonic vibrational frequencies at the same level as a minimum with all positive frequencies or as a transition state with only one imaginary frequency. Frequency calculations without scaling also provided the thermodynamic quantities such as the zero-point vibrational energy (ZPVE), absolute entropy, and thermal corrections to energy, enthalpy, and Gibbs free energy. Transition state structures were located using the Berny algorithm[66] and then verified with intrinsic reaction coordinate (IRC)[67] calculations at the same level of theory. To refine the electronic energies, the optimized geometries obtained by B3LYP/6-31G(d,p) were subjected to the single-point calculations at the B3LYP/6-311++G(d,p) and BB1K/6-311++G(d,p) levels.[63,68,69] BB1K is an abbreviation for Becke88-Becke95 1-parameter model for kinetics. This new hybrid Hartree-Fock density has shown to be an accurate and efficient method for computational kinetics.[69–71] In addition, Solvent effects were tested with the self-consistent reaction field (SCRF) method based on the integral equation formalism polarized continuum model (IEFPCM).[72–75] In this work, single-point energy calculations at the IEFPCM-B3LYP/6-311++G(d,p) and IEFPCM-BB1K/6-311++G(d,p) levels were performed in heptane on the basis of the gas-phase optimized geometries. The default dielectric constant implemented in the program and the atomic radii from the UFF force field were taken for heptane. Both zero-point vibrational energies and thermal corrections at 298.15 K and 1 atm obtained at the B3LYP/6-31G(d,p) level were used to correct electron energies of single-point calculations. Note that, unless otherwise stated, the optimized geometries at the B3LYP/6-31G(d,p) level and

SCHEME 3: Three Possible Reaction Pathways of the Aminolysis Mechanism

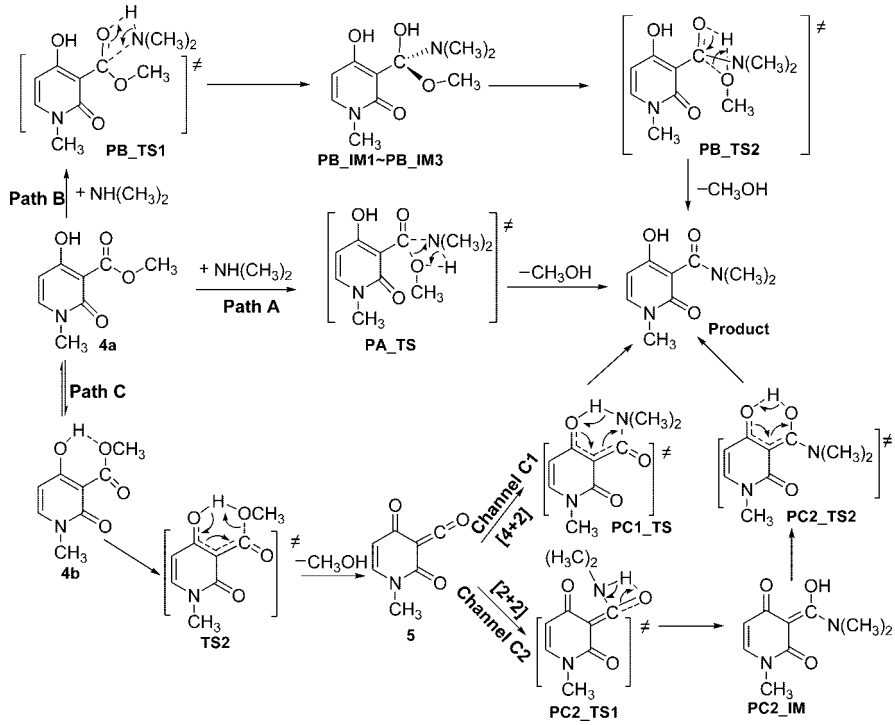

the single-point energies at the B3LYP/6-311++G(d,p) and BB1K/6-311++G(d,p) levels with ZPVE and thermal corrections are reported in this article.

3. Results and Discussion

As presented in Scheme 3, we considered three possible reaction pathways, denoted as paths A, B, and C. Path A is concerted, and paths B and C are stepwise. Similar to the proposed pathways in literatures, paths A and B are also conventional. For path C, the intermediate α-oxo ketene is at first generated from the decomposition of *N*-methyl-3-(methoxycarbonyl)-4-hydroxy-2-pyridone with the participation of *β*-hydroxy, and then the addition of dimethylamine to α-oxo ketene should lead to the product via the [4+2] or [2+2] reaction. All of relative energies are shown in Table S1 in the Supporting Information.

3.1. Concerted Mechanism (Path A). In this pathway, the reaction, involving the nucleophilic attack of the N atom of dimethylamine to the carbonyl C atom of ester and the simultaneous proton transfer from dimethylamine to the oxygen atom of the C−O single bond of ester, is concerted via one transition state **PA_TS**. The corresponding geometries, **PA_RC, PA_TS**, and **PA_PC**, are presented in Figure 1. The transition state **PA_TS** is a four-membered ring structure. The vector of the imaginary vibrational frequency of **PA_TS** is mainly associated with the motion of $H_1$from N_1 to O_2, resulting in the partial formation of the C_3-N_1 bond and the partial cleavage of the C_3-O_2 bond. The distance of C_3-O_2 is 1.9341 Å, which is 0.6018 Å longer than that in **PA_RC** (1.3323 Å). The C_3-N_1 bond length is 1.5512 Å in **PA_TS**, which is 0.1942 Å longer than that in **PA_PC** (1.3570 Å). Figure 2 indicates that, relative to the separate reactants, the energy barrier of **PA_TS** is 40.26 and 39.30 kcal/mol with B3LYP and BB1K methods, respectively.

3.2. Neutral Stepwise Mechanism through Tetrahedral Intermediates (Path B). This possible pathway is actually an addition/elimination process: the hydrogen atom at first transfers from the N atom of dimethylamine to the oxygen atom of the C═O double bond of ester to form a neutral tetrahedral intermediate; then the intermediate slightly adjusts its geometry by rotating some groups to offer a favorable structure to proceed the elimination step; finally the reaction produces amide and methanol. All of relevant structures are presented in Figure 3.

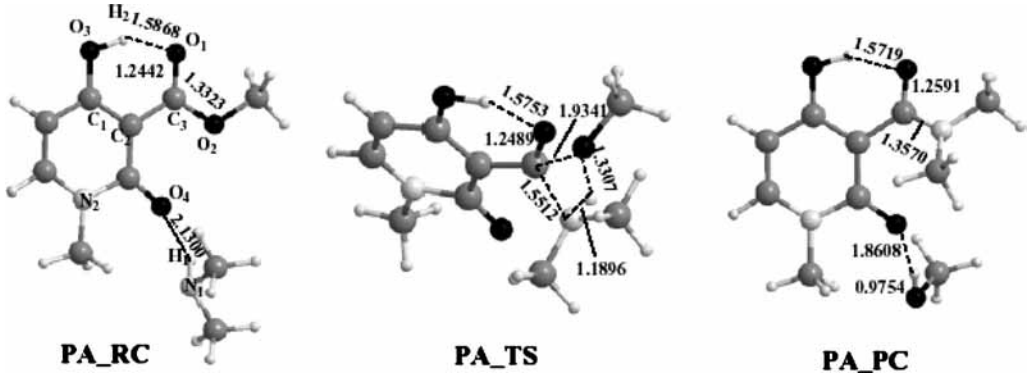

Figure 1. Optimized structures (bond length in Å) in path A at the B3LYP/6-31G(d,p) level.

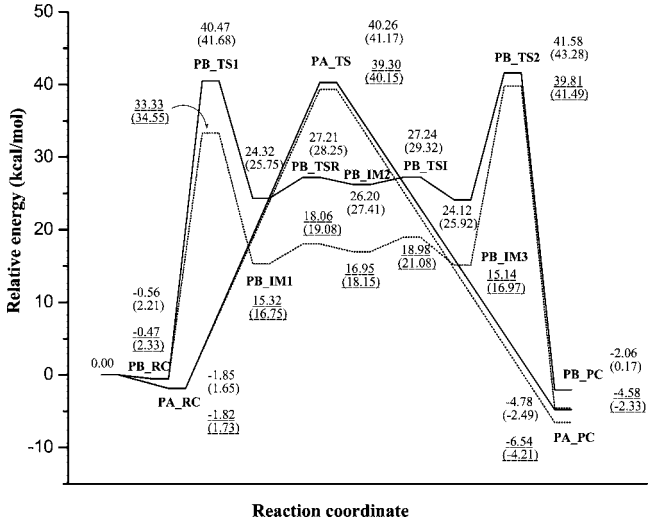

Figure 2. Relative energy profiles (kcal/mol; energies in heptane, in parentheses) for paths A and B using B3LYP (solid line) and BB1K (underlined value, dashed line) methods.

The addition of the N_1-H_1 bond of dimethylamine to the $C_3=O_1$ double bond of ester takes place via the four-membered transition state **PB_TS1**. The distances of C_3-N_1, N_1-H_1, $O_1-H_1$and O_1-C_3 are 1.5824, 1.2920, 1.2557 and 1.3850 Å, respectively. The vector of the imaginary vibrational frequency for **PB_TS1** mainly corresponds to the proton (H_1) transfer from N_1 to the O_1. In the intermediate **PB_IM1**, the hybridization of the electrophilic carbonyl C_3converted from sp^2 in **PB_RC** to sp^3; the $C_3=O_1$ double bond became a single bond (1.2500 Å in **PB_RC** vs 1.4462 Å in **PB_IM1**) with the proton transfer from N_1 to O_1; the C_3-N_1bond simultaneously formed with the length of 1.4703 Å. Note that the dihedral angle of $O_2C_3O_1H_1$ is −94.72°, which implies that H_1 cannot effectively transfer to the lone pair of O_2. To give a favorable geometry to eliminate methanol, we found two more steps between **PB_IM1** and **PB_IM3**. As shown in Figure 3, after the rotation around the C_3-O_1 bond, the intermediate **PB_IM1** changes into the intermediate **PB_IM2** through the transition state **PB_TSR**, leading to the change of the dihedral angle $O_2C_3O_1H_1$ to 38.87° in **PB_IM2**. The intermediate **PB_IM3** is another isomer of **PB_IM2** via **PB_TSI** by the inversion of amino group. From **PB_IM2** to **PB_IM3**, the dihedral angles of $O_1C_3O_2C_4$, $O_1C_3N_1C_5$, and $O_1C_3N_1C_6$ change from +69.97° to −177.67°, +46.84° to −57.14°, and +178.09° to +73.94°, respectively. In the process where the two methyl groups attached at N_1 in **PB_IM2** invert to form **PB_IM3**, the methyl group attached at O_2 also rotates around the C_3-O_2 bond to reduce the spatial repulsion.

In the next step, methanol could be eliminated from **PB_IM3** to form the product complex **PB_PC** via the transition state **PB_TS2**. For **PB_TS2**, the analysis of the vibrational frequency indicates that it mainly corresponds to the proton transfer of H_1 from O_1 to O_2. As shown in Figure 3, the distances of C_3-O_2, H_1-O_1, H_1-O_2 and C_3- O_1 are 1.8961, 1.1171, 1.3399, and 1.3742 Å, respectively; the dihedral angle $C_2C_3O_1N_1$ is 148.95°. Note that the C_3-O_1 and C_3-N_1 bond lengths are 1.3742 and 1.3353 Å, indicating that C_3-O_1 bond partially restores to a double bond and that the N_1 atom partially conjugates with C_3-O_1. Compared with **PB_IM3** and **PB_PC**, we deem that **PB_TS2** is a product-like transition state.

The calculated energies, relative to the sum of energies of separated reactants, are also illustrated in Figure 2. There are two high peaks (**PB_TS1**and **PB_TS2**) on the potential energy surface. Energy barriers of **PB_TS1** and **PB_TS2** are 40.47 and 41.58 kcal/mol with the B3LYP method, respectively. The energy barriers of the rotation (**PB_TSR**) and the inversion (**PB_TSI**) are so low that it is free to generate the favorable geometry **PB_IM3**. Similarly, including the correction by single-point calculations using the BB1K method, we found that, although the relative energy barriers are lower than those of B3LYP, the trend is the same to that of B3LYP. As shown in Figure S1 in the Supporting Information, the relative Gibbs free energy barriers betray that the concerted and the neutral stepwise pathways are very competitive for the title reaction due to the very close free energy barriers in the rate-determining steps. Our findings are also in agreement with some other studies.[12,17,19]

3.3. Stepwise Pathway via α-Oxo Ketene Intermediate (Path C). Herein we will theoretically clarify the unclear pathway (path C) via the intermediate α-oxo ketene, which is different from the conventional aminolysis of *N*-methyl-3-(methoxycarbonyl)-4-hydroxy-2-pyridone with dimethylamine via paths A and B. In this pathway, it should be divided into two sequential processes. The first process is to generate the intermediate α-oxo ketene from the decomposition of *N*-methyl-3-(methoxycarbonyl)-4-hydroxy-2-pyridone; the second process is the attack of the nitrogen atom of amine to the carbon atom of ketenyl group followed by the proton transfer from amine directly or indirectly to α-oxygen to offer amide. Due to the special geometry of α-oxo ketene, we have tested two channels in the second process (channels C1 and C2). Channel C1 is a concerned [4+2] pseudopericyclic addition pathway, and channel C2 is a stepwise pathway including the [2+2] addition and the proton transfer. All of the critical points of this pathway are presented in Figure 4, and the corresponding relative reaction energies are shown in Table S1 and Figure 5.

(1) Decomposition of β-Hydroxy-α,β-Unsaturated Ester To Form α-Oxo Ketene Intermediate. As shown in Scheme 4, one can clearly see that there may be two possibilities, the retro-[2+2] reaction and the retro-[4+2] reaction, to generate the intermediate α-oxo ketene. The retro-[2+2] reaction is the reverse process of [2+2] reaction from keto tautomer of *β*-hydroxy esters **4c**, whereas the retro-[4+2] reaction is the reverse process of [4+2] pseudopericyclic reaction from enol tautomer of *β*-hydroxy esters **4b**. Which one is the more probable mechanism for the formation of α-oxo ketene from *β*-hydroxy esters? All experimental evidences suggested that the retro-[4+2] pathway should be more reasonable than the retro-[2+2] pathway.[30,38] For our system, because the conjugation of hydroxy with pyridone in **4a** is destroyed in *β*-keto tautomer **4c**, *β*-keto tautomer **4c** is less stable than enol tautomer **4a** by ca. 16.01 kcal/mol at the B3LYP/6-311++G(d,p) level. Moreover, the energy barrier from **4a** to **4c** is 67.37 kcal/mol at the B3LYP/6-311++G(d,p) level, and the second step from **4c** to α-oxo ketene is 65.45 kcal/mol at the B3LYP/6-311++G(d,p) level. Such higher barriers suggest that the retro-[2+2] reaction toward α-oxo ketene is somewhat difficult to occur in this decomposition process. Therefore it seems safe to claim that the intermediate α-oxo ketene should be generated via the retro-[4+2] mechanism in the decomposition of *N*-methyl-3-(methoxycarbonyl)-4-hydroxy-2-pyridone.

Due to the fact that **4a** is more stable than **4b** and that **4b** is favorable to undergo the retro-[4+2] reaction, **4a** should firstly convert to **4b** via the transition state **TS1**. In **TS1**, the $O_1C_3O_2$ plane is almost perpendicular to the pyridone ring. To generate the complex **5** via the retro-[4+2] reaction, as shown in Figure 4, we have located the six-membered transition state **TS2**. Analysis of the imaginary frequency showed that the reaction

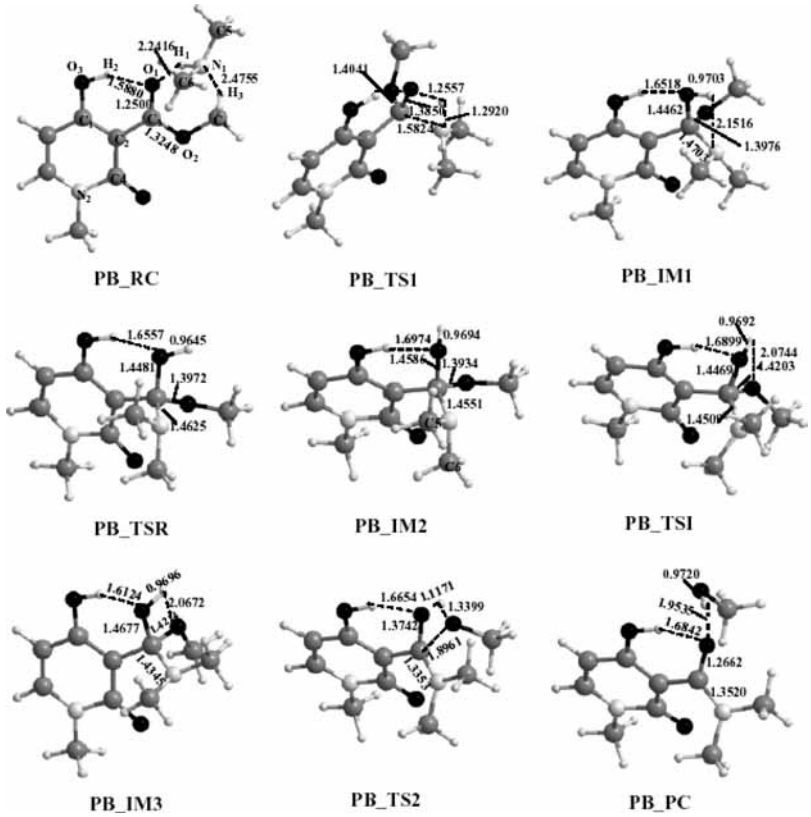

Figure 3. Optimized structures (bond length in Å) in path B at the B3LYP/6-31G(d,p) level.

coordinate vector should be assigned to the coupling of the cleavages of the O_2-C_3 and O_3-H_2 bonds and the formation of the H_2-O_2 bond. The H_2-O_2 bond length is 0.9829 Å in **TS2**, which is 0.0072 Å longer than that in **5**, but 1.1041 Å shorter than that in **4b**. The distances of O_3-H_2 and O_2-C_3 are 1.7223 and 2.4709 Å, which are 0.1193 and 0.3121 Å shorter than those in **5**, but 0.7397 and 1.0752 Å longer than those in **4b**, respectively. The angle $C_2-C_3-O_1$ in **TS2** is 165.93°, very close to that in **5** (174.17°). Accordingly, in view of the structure, **TS2** is a product-like and synchronous transition state. Relative to reactants, as shown in Figure 5, the energy barrier of **TS2** is 28.44 and 35.08 kcal/mol with B3LYP and BB1K methods, respectively, and the relative energy of **5** is 28.05 and 34.30 kcal/mol, respectively. Therefore, this process is strongly endothermic in the gas phase and it turns out that α-oxo ketene is not stable and very active because of the small energy difference between the transition state **TS2** and the complex **5**. However, after amine interacts with complex **5**, the tight complex **PC1_RC** can be generated without energy barrier (detailed results are presented in the next subsection). That is to say, without the addition of amine, it is easy to undergo the backward reaction.

In fact, amine also exists in the experimental process. Therefore, we have also taken into account dimethylamine in our calculations and reinvestigated the process stated above. Here, the complex formed between **4b** and dimethylamine is denoted as **4b′**, and the complex of α-oxo ketene**,**methanol, and dimethylamine is labeled as **5′**. We located the corresponding transition state **TS2′**. The analysis of the imaginary vibrational frequency indicates that the vibrational mode is very similar to that of **TS2**. As stated above, **PC1_RC** can be generated via **TS2,** Therefore, can **PC1_RC** also be generated from **TS2′**? We found, although it is difficult to directly get the answer from the vibrational mode of **TS2′**, IRC results (Figure 6) actually show that **PC1_RC** can be isolated from **5′**, which is directly generated from **TS2′**. From Figure 6, one can clearly see that the detachment of methanol from ester occurs much earlier than the formation of the N1−C3 bond. That is to say, processes with and without amine are almost the same to each other. Compared with **TS2**, the energy barrier of **TS2′** decreases by only 0.39 and 0.93 kcal/mol with B3LYP and BB1K methods, respectively. However, taking into account the contributions of entropies, as shown in Figure S2 in the Supporting Information, the Gibbs free energy barriers of **TS2** and **TS2′** are distinct. The free energy barrier of **TS2′** is about 10 kcal/mol higher than that of **TS2**, indicating that the monomolecular decomposition of **4a** via **TS2** is a favored pathway.

(2) Concerted [4+2] Pseudopericyclic Addition of Dimethylamine to α-Oxo Ketene: Channel C1. In this section, we will present the addition process of dimethylamine to the C═O double bond of α-oxo ketene. In our calculations, methanol was not included explicitly because it was removed from reaction system in the experiment. From Figure 7, one can see that this step corresponds to a concerted [4+2] pseudopericyclic addition. In this step, we at first obtained a tight prereactive complex **PC1_RC** with the $N_1H_1\cdots O_3$ hydrogen bond length of 1.3895 Å. This strong hydrogen bond leads to elongation of the N_1-H_1 bond length to 1.1273 Å. The C_2-C_3-O_1 angle is deviated by ca. 47° from linearity. Then we located the transition state **PC1_TS**. The vector of the imaginary vibrational frequency of **PC1_TS** is associated with the motion of H_1 transfer from N_1 to O_3, which is different from that of the retro-[4+2] transition state **TS2**. The distances of O_3-H_1 and N_1-H_1 are 1.2515 and 1.2228 Å, respectively. For the product complex **PC1_PC**, it has an $O_3H_1\cdots N_1$ hydrogen bond with the length of 1.9572 Å. The distance of the C_3-N_1 bond is 1.4180 Å, which is 0.1270 Å shorter than that in **PC1_TS**. Note that, in this step, C_1, C_2, C_3, N_1, H_1, and O_3 are almost on the same plane. To understand

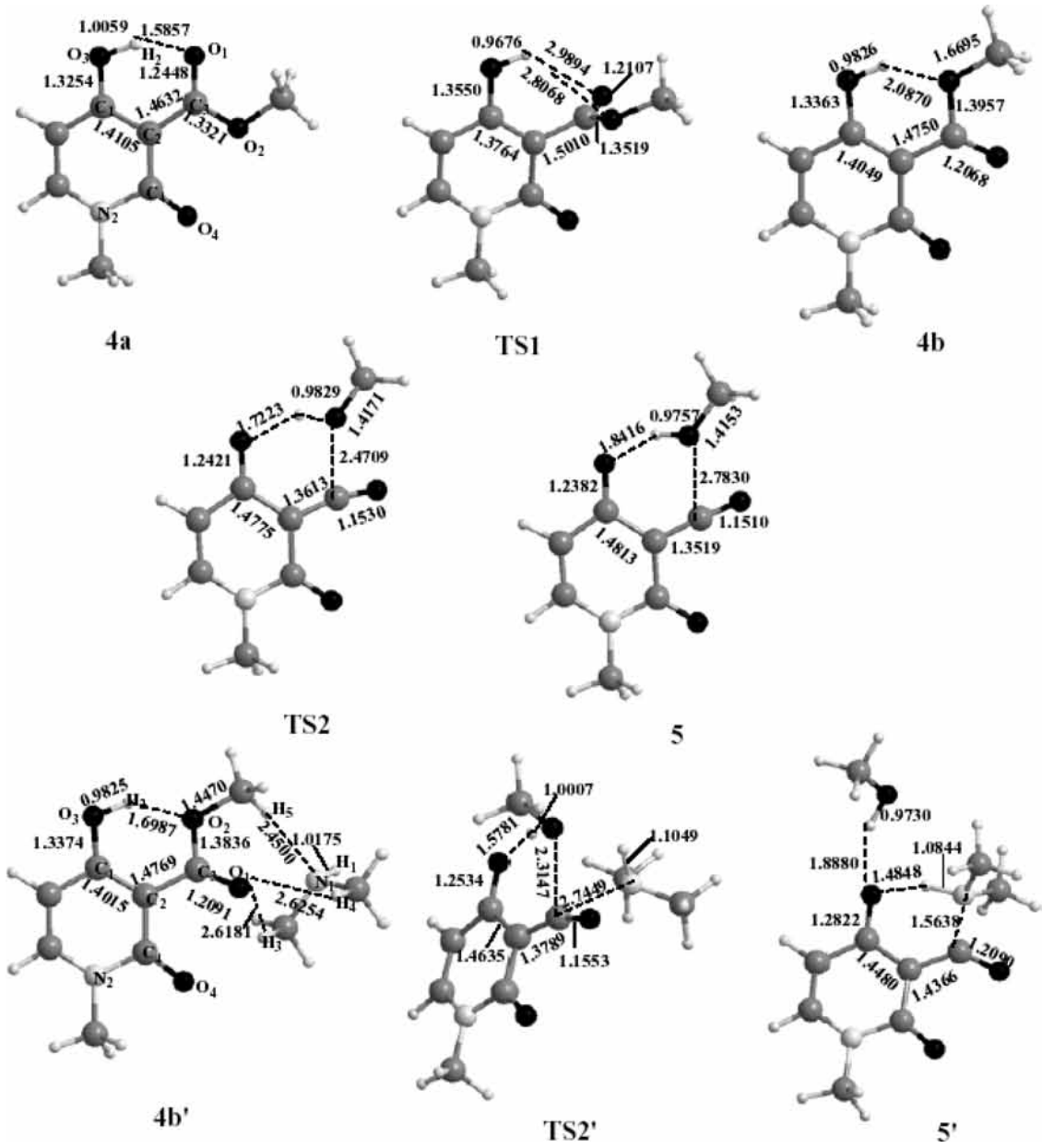

Figure 4. Optimized structures (bond length in Å) in the first step of path C at the B3LYP/6-31G(d,p) level.

why dimethylamine attacks the C_3 atom in a plane not above the plane, two relevant π^* orbitals of a simple α-oxo ketene are shown in Scheme 5. As we know, for propadiene, the hybridization of the central carbon atom is sp and there are two pairs of π bond. The two π bonds are perpendicular to each other. However, for α-oxo ketene, one of π bonds conjugates with the α-position $C_1{=}O_3$ double bond and one lone pair of the ketenyl oxygen to form a more delocalized π bond. Therefore, in our study, there are two choices for dimethylamine to attack the central C_3. If this step undergoes the conventional 1,4-addition reaction, dimethylamine should at first attack the C_3 atom above the molecular plane with the $\pi^*(2)$ orbital, leading to the deviation of the O_1 atom from the plane and thus weakens the delocalized π bond, but the hydrogen atom H_1 could not favorably head to the lone pair of O_3. Alternatively, if dimethylamine attacks the C_3 of the $C_3{=}O_1$ double bond with the $\pi^*(1)$ orbital in the molecular plane, the hydrogen atom H_1 could be favorably head to the lone pair of O_3, the O_1 atom should bend from linearity in the same plane, which could also maintain the conjugation of the $C_3{=}O_1$ double bond with the

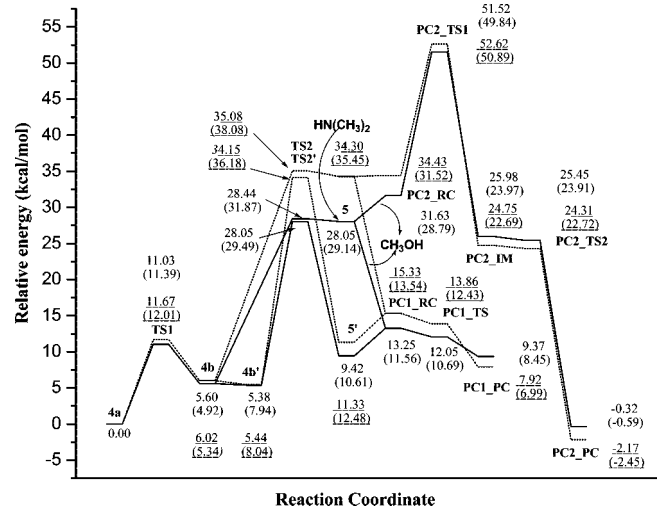

Figure 5. Relative energy profiles (kcal/mol; energies in heptane, in parentheses) for path C using B3LYP (solid line) and BB1K (underlined value, dashed line) methods.

SCHEME 4: Genergation of α-Oxo Ketene via the Retro-[4+2] and Retro-[2+2] Cycloreversions

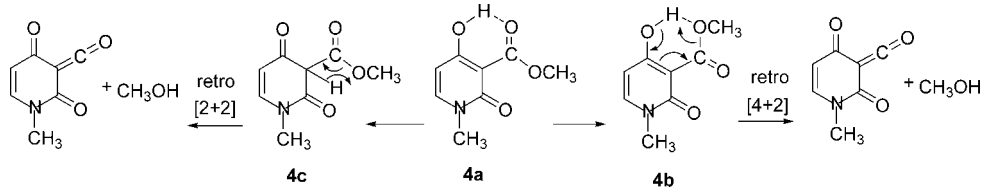

pyridone ring. Taking this into account, we think that it is more rational for dimethylamine to attack at the π bond of the $C_3{=}O_1$ double bond of ketene in the molecular plane. In addition, we guess there may be a transition state to form the tight complex **PC1_RC** from the separated reactants. Unfortunately, we failed to locate that transition state and realized that this step is barrierless although this step should be considered as the process of the nucleophilic attack.

As presented in Figure 5, the relative energy barrier of **PC1_TS** is 12.05 and 13.86 kcal/mol with B3LYP and BB1K methods, respectively, and the relative energy of **PC1_RC** is 13.25 and 15.33 kcal/mol, respectively. It implies that the energy of **PC1_TS** is lower than that of **PC1_RC** with the thermal correction and ZPVE. That is to say, the transition state **PC1_TS** disappears and the complex **PC1_RC** cannot stably exist in the gas phase. Inversely, at the B3LYP/6-311++G(d,p) level, it needs about 19 kcal/mol to form α-oxo ketene by the removal of an amine from amide **PC1_PC**, which is lower than that of **4a** by the removal of a methanol (28.44 kcal/mol). Under the BB1K calculations, the trend is also the same. So, if methanol is in high concentration in the reaction, the equilibrium should favor **4a** and amide **PC1_PC** might be generated in low yield. Of course, if a primary amine such as aniline is used as a trapping nucleophile, the situation should be changed because the reactivity of the primary amine is greater than that of methanol. In this way, the equilibrium is mostly controlled by the thermodynamic factor and methanol has little effect on the equilibrium. In fact, in the experiment, methanol was removed from the reaction system by distillation when the secondary amine was used, but methanol was not removed from the reaction system when the primary amine was used, which indicates that the methanol concentration could have an effect on the reaction equilibrium under different conditions.

(3) Stepwise [2+2] Addition of Dimethylamine to α-Oxo Ketene: Channel C2. In this channel, the reaction at first undergoes the [2+2] addition of dimethylamine to the C═O double bond of the ketenyl group to form an enol amide intermediate. Note that this [2+2] reaction is different from the most common [2+2] reactions of ketenes. Due to the strong conjugation of ketene with the pyridone ring, we think that it is difficult to follow the [2+2] reaction at the C═C double bond of ketene. Therefore, that process was excluded from our calculations. As shown in Figure 7, the prereactive complex **PC2_RC**, transition state **PC2_TS1** and **PC2_TS2**, the intermediate **PC2_IM**, and the product complex **PC2_PC** have been located at the B3LYP/6-31G(d,p) level in the gas phase. The corresponding energies are also presented in Figure 5. **PC2_TS1** is a four-membered ring structure. The vector of the imaginary vibrational frequency for **PC2_TS1** is mainly corresponding to the mode of the proton (H_1) transfer from N_1 of dimethylamine to the carbonyl O_1 of α-oxo ketene. The $C_3{-}N_1$and $O_1{-}H_1$ bond lengths are 1.4995 and 1.2669 Å, respectively. It can be found that the transition state **PC2_TS1**, in which the central carbon of the ketenyl group has strongly bonded to the N_1 atom of the nucleophile, is concerted but asynchronous. After the reaction overcame the **PC2_TS1**, the intermediate enol amide **PC2_IM** is generated. In **PC2_IM**, the $C_3{-}N_1$ and $O_1{-}H_1$ bond lengths are 1.3483 and 0.9689 Å, which are 0.1512 and 0.2980 Å shorter than those in **PC2_TS1**, respectively. Next, we found that amide complex **PC2_PC** can directly be produced via the transition state **PC2_TS2**. Because the structures of **PC2_IM** and **PC2_TS2** are very similar to each other, **PC2_TS2** is reactant-like and should be an early transition state. The vector of the imaginary vibrational frequency for **PC2_TS2** is mainly corresponding to the rotational mode of the $O_1{-}H_1$ bond around the $C_3{-}O_1$ bond. Figure 5 indicates that the relative activation energy of the first step is 51.52 and 52.62 kcal/mol under the B3LYP and BB1K calculations, respectively, and the second step is also a barrierless process.

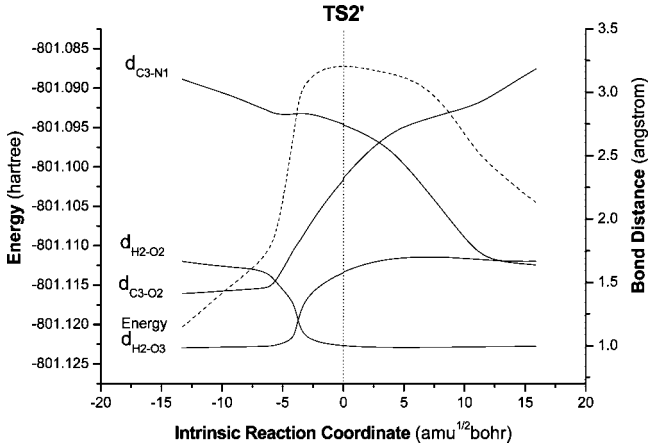

Figure 6. Changes of some selected bond distances (angstrom) along the potential energy profile from **4b′** to **5′** via **TS2′** at the B3LYP/6-31G(d,p) level.

In path C Figure 5 indicates that the relative energies at the BB1K/6-311++G(d,p) level are comparable with those at the B3LYP/6-311++G(d,p) level with the exception of **TS2** and **TS2′** in which relative energies increase about 6 kcal/mol using the BB1K method. As mentioned above, in the energy point of view, it turns out that channel C1 is very favorable for the second process of the mechanism via α-oxo ketene (path C). Therefore, for the title reaction, the first step is to form α-oxo ketene, which is a rate-limiting step, and then the second step is to produce **PC1_PC** via channel C1, which is a [4+2] pseudopericyclic addition process. In all, taking into account the three pathways, paths A, B and C, we can conclude that path C has the highest possibility to occur in the aminolysis of *N*-methyl-3-(methoxycarbonyl)-4-hydroxy-2-pyridone.

Jansson et al.[21] found that the rate of the reaction obeys the first-order rate law, which obviously exhibited that the reaction should include a unimolecular rate-determining step. From our results, because the second step (channel C1) is barrierless and the transition state for the generation of α-oxo ketene is independent of amine in path C, the first step, which produces the intermediate α-oxo ketene, is the rate-limiting step and thus

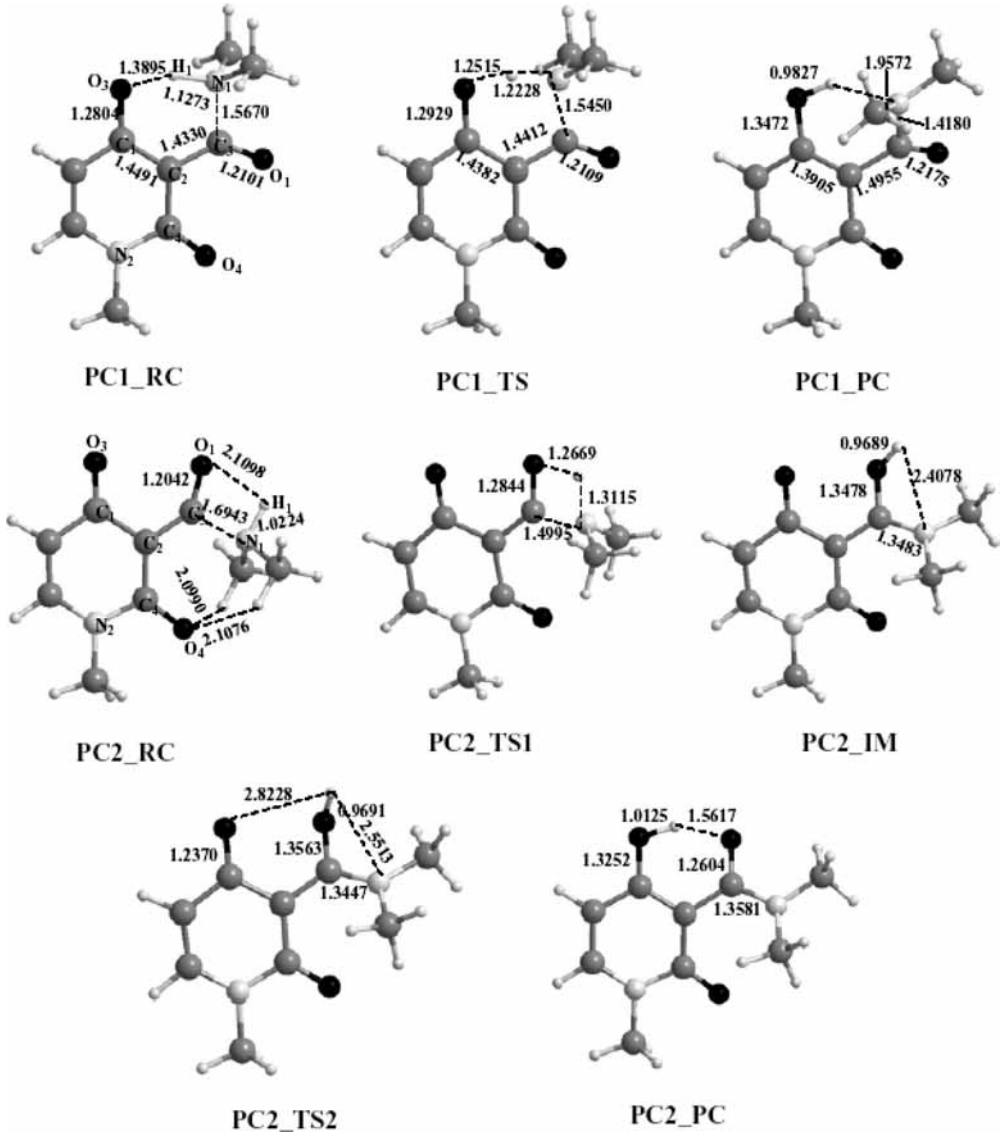

Figure 7. Optimized structures (bond length in Å) in the second step of path C at the B3LYP/6-31G(d,p) level.

SCHEME 5: Two Relevant π^* Orbitals and Energies for the Simple α-Oxo Ketene at the B3LYP/6-31G(d,p) Level

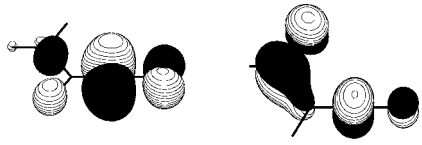

obeys the first-order rate law, which is in good agreement with the experimental results.

3.4. Solvent Effects. Furthermore, to take into account the solvent effects on the title reaction, we have performed the single-point calculations at the IEFPCM-B3LYP/6-311++G(d,p)//B3LYP/6-31G(d,p) and IEFPCM-BB1K/6-311++G(d,p)//B3LYP/6-31G(d,p) levels for all gas-phase optimized stationary points. To mimic the solvent effects in the experiment, heptane has been taken as solvent in our calculations. Recently, Lithoxoidou and Bakalbassis76 theoretically studied some aromatic compounds in the gas phase and solvents, and found that some solvents (dielectric constant <30) have little effect on the gas-phase geometries (differences in bond distances <0.004 Å, differences in angles <1.5°). Accordingly, it is rational to conduct the single-point energy computations in heptane (ϵ =1.92) using the gas-phase optimized geometries. The corresponding energies are also presented in Figures 2 and 5. We found that solvation energies under the B3LYP and BB1K method are almost the same. The results indicate that, in heptane, both the energy barriers of the rate-determining step in paths A and B slightly increase by ca 1.0 kcal/mol at the two DFT methods, and that the precursor (complexes **PA_RC** and **PB_RC**) cannot be formed due to the instability of these structures in heptane. For path C, under the B3LYP and BB1K computations in heptane, the energy barrier of the rate-limiting step is 29.49 and 36.18 kcal/mol, respectively, and the free energy barrier is 26.72 and 33.40 kcal/mol, respectively; the second step (channel C1) is also barrierless in heptane. Birney et al.[33] reported that the addition of amine to formylketene was also a barrierless process at the MP4(SDQ)/6-31G*+ZPE//MP2/6-31G* level, which can strongly support our results.

From Figures 2 and 5, because heptane exhibits little solvent effects, the mechanism and the energetics are very similar in the gas phase and in heptane. Of three possible reaction pathways, path C via channel C1 is the most favorable for the title reaction both in the gas phase and in heptane.

Note that formation of a complex from the separated reactants results in a decrease in entropy, leading to an increase in the Gibbs free energy. In our system, as shown in Table S1, Figure S1 and Figure S2, contribution of $-T\Delta S$ is ca. 8 kcal/mol in forming of the complexes. However, the binding energies of the complexes are lower than 8 kcal/mol, which implies that, taking into account the contributions of entropies, the complexes could not be formed both in the gas phase and heptane.

4. Conclusion

The B3LYP/6-31G(d,p) level of theory was applied to optimize all of the stationary points of the aminolysis of *N*-methyl-3-(methoxycarbonyl)-4-hydroxy-2-pyridone with dimethylamine. Single-point computations have also been conducted at the B3LYP/6-311++G(d,p) and BB1K/6-311++G(d,p) levels, based on the geometries optimized at the B3LYP/6-31G(d,p) level. These two hybrid DFT methods give the similar results in this work. Among the several reaction pathways, the most favorable one is to form α-oxo ketene intermediate via the retro-[4+2] pseudopericyclic pathway and then followed by channel C1 to offer the target product (path C). Our results showed that the decomposition of *N*-methyl-3-(methoxycarbonyl)-4-hydroxy-2-pyridone to form α-oxo ketene and methanol is the rate-determining step with $\Delta G^{\neq}$ of 25.66 and 32.30 kcal/mol with B3LYP and BB1K methods in the gas phase. The title reaction, independent of amine concentration in **TS2**, obeys the first-order rate law. To examine the solvent effects on the energies and the mechanism, we have performed single-point calculations at the IEFPCM-B3LYP/6-311++G(d,p) and IEFPCM-BB1K/6-311++G(d,p) levels in heptane, and found that heptane has little effect on the reaction mechanism.

Acknowledgment. This project has been supported by the National Natural Science Foundation of China (Grant Nos. 20773089, 20473055, 20725312, and 20533060), the Ministry of Science and Technology (2007CB815201) and the Scientific Research Foundation for the Returned Overseas Chinese Scholars, State Education Ministry (Grant No. 20071108-18-15).

Supporting Information Available: Complete ref 62. Listings of Cartesian coordinates and energies in hartrees at the B3LYP/6-31G(d,p) level for all critical structures, relative energies (Table S1), and relative free energies profiles (Figures S1 and S2). This material is available free of charge via the Internet at http://pubs.acs.org.

References and Notes

(1) Rogers, G. A.; Bruice, T. C. *J. Am. Chem. Soc.* **1974**, *96*, 2473.
(2) Williams, A. *Acc. Chem. Res.* **1989**, *22*, 387.
(3) Um, I. H.; Min, J. S.; Ahn, J. A.; Hahn, H. J. *J. Org. Chem.* **2000**, *65*, 5659.
(4) Castro, E. A.; Andujar, M.; Campodonico, P.; Santos, J. G. *Int. J. Chem. Kinet.* **2002**, *34*, 309.
(5) Um, I. H.; Lee, S. E.; Kwon, H. J. *J. Org. Chem.* **2002**, *67*, 8999.
(6) Castro, E. A.; Andujar, M.; Toro, A.; Santos, J. G. *J. Org. Chem.* **2003**, *68*, 3608.
(7) Oie, T.; Loeew, G. H.; Burt, S. K.; Binkley, J. S.; Mcelroy, R. D. *J. Am. Chem. Soc.* **1982**, *104*, 6169.
(8) Wang, L.; Zipse, H. *Liebigs Ann.* **1996**, 1501.
(9) Zipse, H.; Wang, L.; Houk, K. N. *Liebigs Ann.* **1996**, 1511.
(10) Marlier, J. F.; Haptonsall, B. A.; Johnson, A. J.; Sacksteder, K. A. *J. Am. Chem. Soc.* **1997**, *119*, 8838.
(11) Adalstensson, H.; Bruice, T. C. *J. Am. Chem. Soc.* **1998**, *120*, 3440.
(12) Yang, W.; Drueckhammer, D. G. *Org. Lett.* **2000**, *2*, 4133.
(13) O'Hair, R. A. J.; Androutsopoulos, N. K. *Org. Lett.* **2000**, *2*, 2567.
(14) Kim, C. K.; Li, H. G.; Lee, H. W.; Sohn, C. K.; Chun, Y. I.; Lee, I. *J. Phys. Chem. A* **2000**, *104*, 4069.
(15) Singleton, D. A.; Merrigan, S. R. *J. Am. Chem. Soc.* **2000**, *122*, 11035.
(16) Ilieva, S.; Galabov, B.; Musaev, D. G.; Morokuma, K.; Schaefer, H. F., III *J. Org. Chem.* **2003**, *68*, 1496.
(17) Ilieva, S.; Galabov, B.; Musaev, D. G.; Morokuma, K. *J. Org. Chem.* **2003**, *68*, 3406.
(18) Ilieva, S.; Atanasov, Y.; Kalcheva, V.; Galabov, B. *J.Mol. Struct. (THEROCHEM)* **2003**, *633*, 49.
(19) Galabov, B.; Atanasov, Y.; Ilieva, S.; Schaefer, H. F., III *J. Phys. Chem. A* **2005**, *109*, 11470.
(20) Rangelov, M. A.; Vayssilov, G. N.; Yomtova, V. M.; Petkov, D. D. *Org. Biomol. Chem.* **2005**, *3*, 737.
(21) Jansson, K.; Fristedt, T.; Olsson, A.; Svensson, B.; Jonsson, S. *J. Org. Chem.* **2006**, *71*, 1658.
(22) Wentrup, C.; Heilmayer, W.; Kollenz, G. *Synthesis* **1994**, 1219.
(23) Tidwell, T. T. *Ketenes II*; John Wiley & Sons, Inc.: Hoboken, NJ, 2006.
(24) Kappe, C. O.; Wong, M. W.; Wentrup, C. *J. Org. Chem.* **1995**, *60*, 1686.
(25) Allen, A. D.; Andaos, J.; Kresge, A. J.; McAllister, M. A.; Tidwell, T. T. *J. Am. Chem. Soc.* **1992**, *114*, 1878.
(26) Zawacki, F. J.; Crimmins, M. T. *Tetrahedron Lett.* **1996**, *37*, 6499.
(27) Zuhse, R. H.; Wong, M. W.; Wentrup, C. *J. Phys. Chem.* **1996**, *100*, 3917.
(28) Chiang, Y.; Guo, H. -X.; Kresge, A. J.; Tee, O. S. *J. Am. Chem. Soc.* **1996**, *118*, 3386.
(29) Koch, R.; Wong, M. W.; Wentrup, C. *J. Am. Chem. Soc.* **1996**, *61*, 6809.
(30) Witzeman, J. S. *Tetrahedron Lett.* **1990**, *31*, 1401.
(31) Witzeman, J. S.; Nottingham, W. D. *J. Org. Chem.* **1991**, *56*, 1713.
(32) Clemens, R. J.; Witzeman, J. S. *J. Am. Chem. Soc.* **1996**, *111*, 2186.
(33) Birney, D. M.; Xu, X.; Ham, S.; Huang, X. *J. Org. Chem.* **1997**, *62*, 7114.
(34) Birney, D. M.; Wagenseller, P. E. *J. Am. Chem. Soc.* **1994**, *116*, 6262.
(35) Birney, D. M.; Ham, S.; Unruh, G. R. *J. Am. Chem. Soc.* **1997**, *119*, 4509.
(36) Liu, R. C.-Y.; Lusztyk, J.; McAllister, M. A.; Tidwell, T. T.; Wagner, B. D. *J. Am. Chem. Soc.* **1998**, *120*, 6247.
(37) Emerson, D. W.; Titus, R. L.; Gonzalez, R. M. J. *Org. Chem.* **1991**, *56*, 5301.
(38) Freiermuth, B.; Wentrup, C. *J. Org. Chem.* **1991**, *56*, 2286.
(39) Gong, L.; McAllister, M. A.; Tidwell, T. T. *J. Am. Chem. Soc.* **1991**, *113*, 6021.
(40) Birney, D. M. *J. Org. Chem.* **1994**, *59*, 2557.
(41) Montero-Campillo, M. M.; Rodriguez-Otero, J.; Cabaleiro-Lago, E. M. *J. Phys. Chem. A* **2004**, *108*, 8373.
(42) Wagenseller, P. E.; Birney, D. M.; Roy, D. *J. Org. Chem.* **1995**, *60*, 2853.
(43) Eisenberg, S. W. E.; Kurth, M. J.; Fink, W. H. *J. Org. Chem.* **1995**, *60*, 3736.
(44) Nguyen, M. T.; Ha, T.; More O'Ferrall, R. A. *J. Org. Chem.* **1990**, *55*, 3251.
(45) Keeffe, J. R. *J. Phys. Org. Chem.* **2004**, *17*, 1075.
(46) Ham, S.; Birney, N. M. *J. Org. Chem.* **1996**, *61*, 3962.
(47) Tidwell, T. T. *Acc. Chem. Res.* **1990**, *23*, 273.
(48) Snider, B. B. *Chem. Rev.* **1988**, *88*, 793.
(49) Ye, T.; McKervey, M. A. *Chem. Rev.* **1994**, *94*, 1091.
(50) Andaos, J.; Kresge, A. *J. Am. Chem. Soc.* **1992**, *114*, 5643.
(51) Kuangsen, S.; Tidwell, T. T. *J. Am. Chem. Soc.* **1998**, *120*, 3043.
(52) Allen, A. D.; Tidwell, T. T. *J. Org. Chem* **1999**, *64*, 266.
(53) Raspoet, G.; Nguyen, M. T. *J. Org. Chem.* **1998**, *63*, 9669.
(54) Acton, A. W.; Allen, A. D.; Antunes, L. M.; Fedorov, A. V.; Najafian, K.; Tidwell, T. T.; Wagner, B. D. *J. Am. Chem. Soc.* **2002**, *124*, 13790.
(55) Wagner, B. D.; Arnold, B. R.; Brown, G. S.; Lusztyk, J. *J. Am. Chem. Soc.* **1998**, *120*, 1827.
(56) Bernardi, F.; Bottoni, A.; Robb, M. A.; Venturini, A. *J. Am. Chem. Soc.* **1990**, *112*, 2106.
(57) Wang, Z.; Houk, K. N. *J. Am. Chem. Soc.* **1990**, *112*, 1754.
(58) Schaad, L. J.; Gutman, I.; Hess, B. A., Jr.; Hu, J. *J. Am. Chem. Soc* **1991**, *113*, 5200.
(59) Seidl, E. T.; Schaefer, H. F., III *J. Am. Chem. Soc.* **1991**, *113*, 5195.
(60) Sordo, J. A.; Gonzalez, J.; Sordo, T. L. *J. Am. Chem. Soc.* **1992**, *114*, 6249.
(61) Ross, J. A.; Seiders, R.P.; Lemal, D. M. *J. Am. Chem. Soc.* **1976**, *98*, 4325.
(62) Frisch, M. J.; *Gaussian 03*, revision D.01; Gaussian, Inc.: Wallingford, CT, 2005. The complete reference is shown in the Supporting Information).
(63) Becke, A. D. *Phys. Rev.* **1988**, *38*, 3098.
(64) Lee, C.; Yang, W.; Parr, R. G. *Phys. Rev. B* **1998**, *37*, 785.

(65) Vosko, S. H.; Wilk, L.; Nusair, M. *Can. J. Phys.* **1980**, *58*, 1200.
(66) Peng, C.; Ayala, P. Y.; Schlegel, H. B.; Frisch, M. J. *J. Comput. Chem.* **1996**, *17*, 49.
(67) Gonzalez, C.; Schlegel, H. B. *J. Chem. Phys.* **1989**, *90*, 2154.
(68) Becke, A. D. *J. Chem. Phys.* **1996**, *104*, 1040.
(69) Zhao, Y.; Lynch, B. J.; Truhlar, D. G. *J. Phys. Chem. A* **2004**, *108*, 2715.
(70) Zhao, Y.; Truhlar, D. G. *J. Phys. Chem. A* **2005**, *109*, 5656.
(71) Zhao, Y.; Gonzalez-Garcia., N.; Truhlar, D. G. *J. Phys. Chem. A* **2005**, *109*, 2012.
(72) Cances, M. T.; Mennucci, B.; Tomasi, J. *J. Chem. Phys.* **1997**, *107*, 3020.
(73) Mennucci, B.; Tomasi, J. *J. Chem. Phys.* **1997**, *106*, 5151.
(74) Mennucci, B.; Cances, E.; Tomasi, J. *J. Phys. Chem. B.* **1997**, *101*, 10506.
(75) Tomasi, J.; Mennucci, B.; Cances, E. *J. Mol. Struct.* **1999**, *464*, 211.
(76) Lithoxoidou, A. T.; Bakalbassis, E. G. *J. Phys. Chem. A* **2005**, *109*, 366.

JP0756496